minerals

MDPI

Article

Results of the Study of Epigenetic Changes of Famennian–Tournaisian Carbonate Rocks of the Northern Marginal Shear Zone of the Caspian Syneclise (Kazakhstan)

Valeriy Korobkin [1,*], Akhan Chaklikov [1,*], Zhamal Tulemissova [1], Iskander Samatov [2] and Yelena Dobrovolskaya [1]

[1] School of Geology, Kazakh-British Technical University, Almaty 050000, Kazakhstan
[2] Institute of Geological Sciences of K.I. Satpayev, Almaty 050010, Kazakhstan
* Correspondence: korobkin_vv@kbtu.kz (V.K.); a.chaklikov@kbtu.kz (A.C.); Tel.: +7-777-136-88-11 (V.K.); +7-701-999-51-10 (A.C.)

Abstract: Various genetic and morphological types of voids in carbonate reservoirs make it difficult to diagnose them, which can be seen in the determination of reservoir properties in the northern marginal shear zone of the Caspian Syneclise. A macro- and microscopic study of rocks was carried out by staining carbonates in thin sections with alizarin (determination of the mineral composition, structure, texture, void and fracture spaces, rock genesis). Instrumental methods (X-ray, DTA—differential thermal analysis, TGA—thermo-gravimetric analysis, and probe microanalysis) established the composition of rocks, the nature of their diagenetic transformations, and the formation of void space. The elemental and oxide composition of a number of samples was carried out using the X-ray probe microanalysis method, and mineral formations with intermediate thermochemical properties were found. The results of X-ray, DTA, and TGA measurements and the data of probe microanalysis made it possible to reveal thermally inert formations of oxides of calcium, magnesium, silicon, iron, and other compounds in the composition of carbonates. A relatively low-cost express method was used to determine the material composition and the nature of epigenetic changes and to obtain data on the void space as a result of the development of tectonic fracturing and diagenetic processes of leaching and secondary mineral formation in bedded carbonate reservoirs.

Keywords: north marginal shear zone; Caspian Syneclise; carbonate reservoir; diagenetic transformations; shear and tension joints; microscopic analysis; X-ray diffractometry; thermal analysis; probe microanalysis

check for updates

Citation: Korobkin, V.; Chaklikov, A.; Tulemissova, Z.; Samatov, I.; Dobrovolskaya, Y. Results of the Study of Epigenetic Changes of Famennian–Tournaisian Carbonate Rocks of the Northern Marginal Shear Zone of the Caspian Syneclise (Kazakhstan). *Minerals* **2023**, *13*, 249. https://doi.org/10.3390/min13020249

Academic Editors: Hamzeh Mehrabi, Vahid Tavakoli and Jia-Xi Zhou

Received: 28 December 2022
Revised: 8 February 2023
Accepted: 8 February 2023
Published: 9 February 2023

Copyright: © 2023 by the authors. Licensee MDPI, Basel, Switzerland. This article is an open access article distributed under the terms and conditions of the Creative Commons Attribution (CC BY) license (https://creativecommons.org/licenses/by/4.0/).

1. Introduction

Carbonate reservoirs play an important role in global hydrocarbon production. The purpose of this study was to select the best methods for studying epigenetic changes in the bedded carbonate reservoirs of the Famennian–Tournaisian reservoirs of the Northern marginal zone of the Caspian Syneclise. Therefore, the primary task for researching these reservoirs is studying the void space and preserving it as a part of the process of further geological evolution. The diversity of genetic types of voids in carbonate rocks determines if a complex reservoir will be created within them. At the early stage of accumulation formation (syngenesis and early diagenesis), a combination of basic parameters such as carbonate deposition depth, oxygen regime, hydrodynamic activity, the composition of seawater and pore water, and the influence of drift sources is important. Subsequent transformations associated with epigenesis are caused by tectonic rearrangements that activate the movements of fluids, including hydrocarbons. As a result of these transformations, the primary structure of the rock can be altered completely [1–6].

The Caspian Syneclise is located in the southeastern part of the East European Craton. Most of its area (about two-thirds) belongs to the Republic of Kazakhstan. The Caspian

Syneclise is a part of the main oil and gas province of the country. The sedimentary cover of the syneclise has a vertical thickness ranging from 6 to 24 km and is subdivided into three lithological-stratigraphic units: (1) pre-salt (Mesoproterozoic–Permian and Artinian stages); (2) saline (Permian and Kungurian stages); and (3) post-salt (Guadalupian section of the Permian–Mesozoic–Cenozoic stage). A characteristic feature of the upper part of the pre-salt section is the presence of an extensive carbonate massif. The reservoirs are carbonate rocks and, mainly, organogenic limestones from the Devonian and Carboniferous age, in which the main oil and gas fields are localized. For a long time, the properties of massive carbonate reservoirs of such known and unique deposits, including the Karachaganak, Tengiz, Kashagan, and Zhanazhol fields, as well as other objects, have been studied (Figure 1) [1,2,4–6]. On the other hand, many deposits that are located in the Chinarevskoye and Lobodin-Teplov groups along the northern border zone of the Caspian Syneclise, which have bedded and bedded–massive reservoirs, have not received enough attention. The objective of our research was to the study the material composition and reservoir properties of carbonate rocks of the northern marginal zone of the Caspian Syneclise.

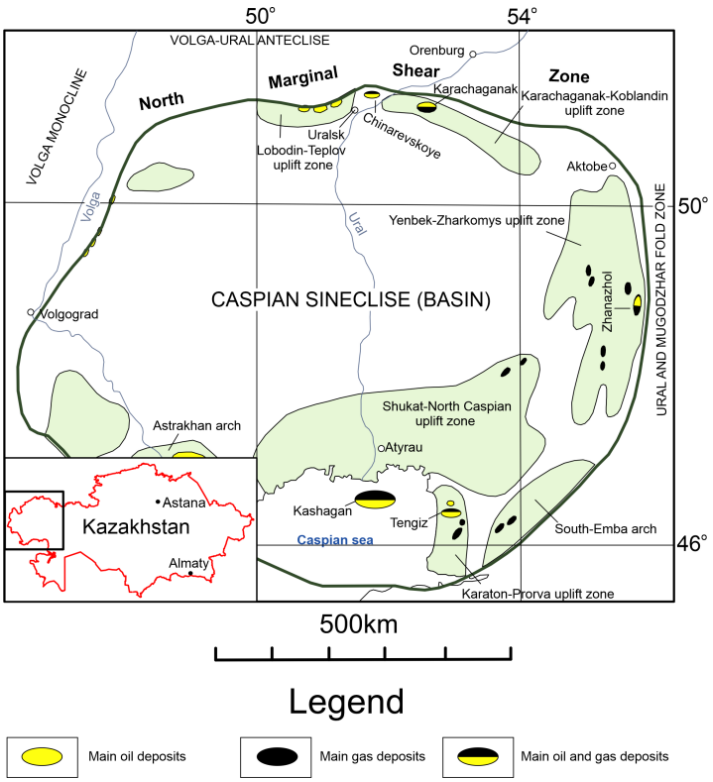


Figure 1. Modified overview diagram of the Caspian Syneclise (Basin) [1,4]. In the northern part of the scheme, there is a northern marginal shear zone separating the Caspian Syneclise from the Volga-Ural Anteclise.

In the outer-edge zone of the northern part of the Caspian Syneclise (oil and gas province), the issues of epigenetic changes of the Famennian–Tournaisian reservoirs can be considered by studying, for example, the Lobodin-Teplov and Chinarevskoye groups of deposits (LTCGD) (Figures 1–3). There are two industrially productive stratigraphic levels of oil and gas content: (1) Givetian–Frasnian gas condensate and (2) Famennian–Tournaisian gas and oil. The trap has a complex combined geological structure. During the Givetian–Tournaisian period, a carbonate formation was formed, which was subsequently converted into an anticline with a complicated sublatitudinal discharge (Figure 2) [5–9].

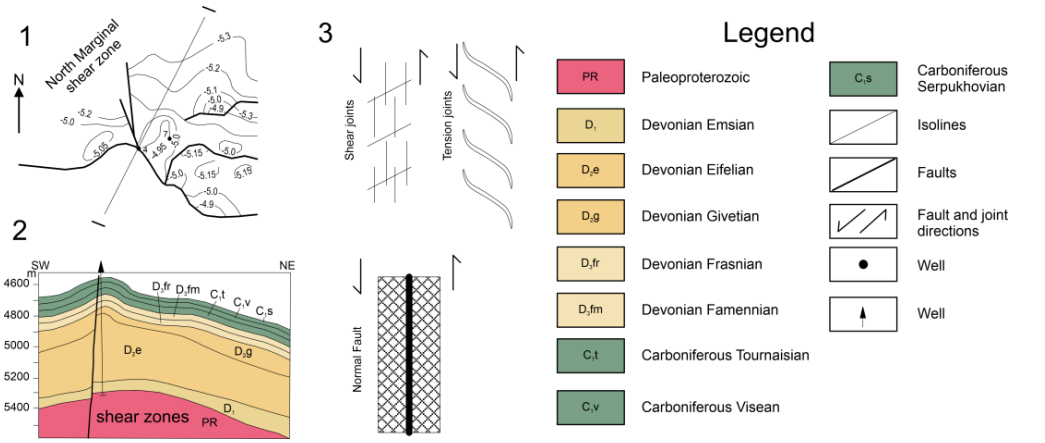


Figure 2. Northern border zone near the Chinarevskoye and Lobodin-Teplov groups: (**1**)—structural diagram; (**2**)—geological section along the I–I line [2]; (**3**)—diagram explaining the formation of joints in the suture zone.

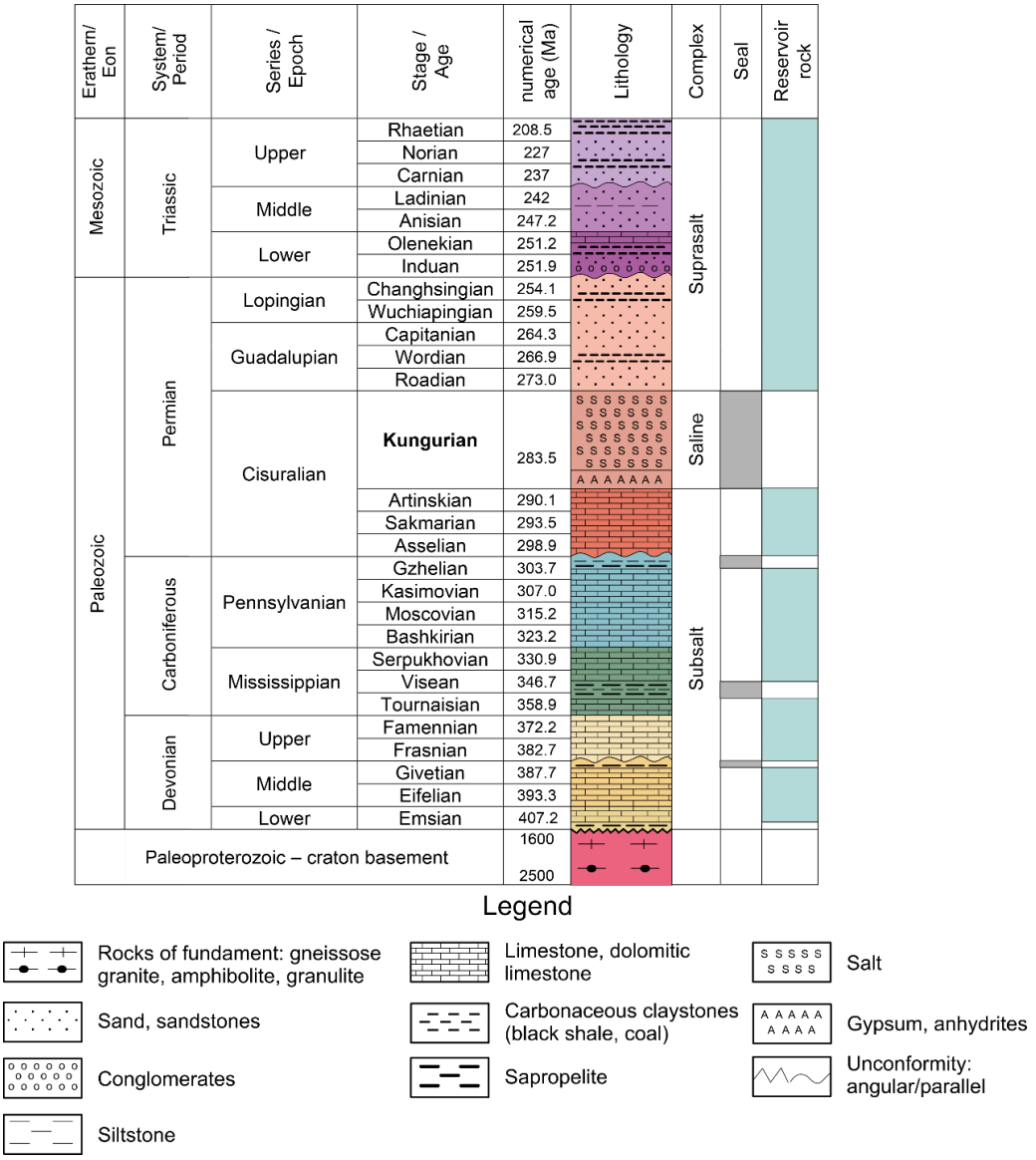


Figure 3. Lithological and stratigraphic diagram of the northern border zone of the Caspian Basin; the modern geochronological edition.

At the LTCGD, the carbonate rocks of the Tournaisian and upper Famennian stages were formed under the conditions of the marine shelf with a variable porosity from 6% to 12%, an average porosity of the gas-saturated part of the reservoir of 8.9%, and an average porosity of the oil-saturated part of up to 8.1%. The Tournaisian oil reservoir with a thin gas cap was discovered and tested in well 10; the GOC was installed at a depth of 4318 m, and the thickness of the gas-bearing stratum is 43 m. The OWC is probably in the range of 4503 m. The established height of the oil reservoir is 77 m, and the effective gas- and oil-saturated thicknesses in the well reach 12.4 m and 61.4 m, respectively [2,10].

In the area of the LTCGD, carbonate sedimentation was carried out on the raised ledge of the foundation, which was formed as a result of the Breton folding phase (according to Hans Stille) that occurred on the border of the Famennian and Tournaisian stages. Fine and coarse clastic sediments accumulated in the depressions surrounding the China–Revskoye uplift. The offshore stage of carbonate offshore sedimentation under the conditions of the passive continental margin of the main basin and subsequent processes created favorable conditions for the development of reservoirs.

In general, the studied reservoir rocks of the Famennian–Tournaisian stage are represented by limestones, dolomites, and calcareous dolomites, with rare inclusions of anhydrite and gypsum. The void space is represented by leaching pores of various shapes and sizes. There are also caverns confined to joints, on the walls of which large dolomite crystals are noted [1,5]. Bioclastic algal limestones with stylolites have widely developed among the rocks. The rocks are fractured (closed joints filled with secondary minerals that are open, subhorizontal, and subvertical), and unevenly porous, as seen in Figure 4. The gross porosity averages 8%–9%.

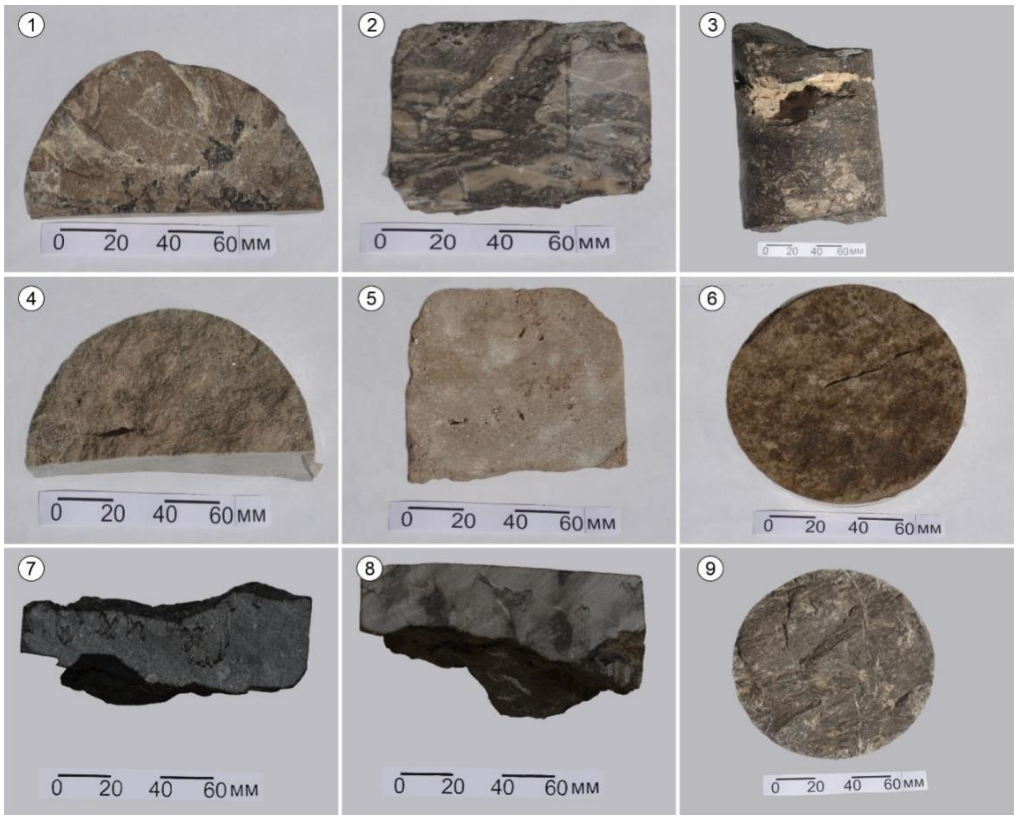


Figure 4. Carbonate reservoirs: (**1**)—limestone, depth of 4390 m; (**2**)—dolomite, depth of 5083–5090 m; (**3**)—dolomite limestone with signs of hydrocarbons, depth of 4943–4952 m; (**4**)—limestone, depth of 4367 m; (**5**)—dolomite, depth of 4616–4621 m; (**6**)—limestone, depth of 2802 m; (**7**)—limestone, depth of 4334 m; (**8**)—limestone, depth of 4390 m (stylolites); (**9**)—limestone, depth of 4924 m.

2. Research Methods

2.1. Macro- and Microscopic Description of Rocks

Macro- and microscopic studies of rocks were carried out for the determination of mineral composition, structure and texture, void space, and rock genesis. The analysis of the reservoir rocks was carried out on R-312 series and Leica FLOORS polarization microscopes (model DMLSP, manufacturer—Leica Microsystems, Wetzlar, Germany). For the diagnosis of carbonates, the staining of a thin section of the carbonates with alizarin red was performed according to the special research method of I. Mitchell [11], allowing us to distinguish calcite from dolomite.

2.2. Instrumental Research Methods

The material composition of the rocks was studied via thermal (DTA and TGA) and X-ray diffractometric analysis methods. Control of the elemental, oxide, and carbon composition of several samples was carried out using radiometric probe microanalysis.

Thermal analysis was carried out on a thermal balance unit: a derivatograph (model: Q-1500D-grade, Budapest, Hungary) created by F. Paulik, J. Paulik, and L. Erdei. The method was based on the device recording changes in the thermochemical and physical parameters of the substance that may be caused by its heating. The thermochemical state of the sample was described by the following curves: T (temperature), DTA (differential thermoanalytical), TG (thermogravimetric), and DTG (differential thermogravimetric, which is a derivative of the TG function). The analysis was performed in the open air, within a temperature range from 20 °C to 1000 °C. The furnace heating mode was linear (dT/dt = 10), and the reference substance was calcined Al_2O_3. The sample weighed strictly 500 mg, with the sensitivity of the balance being 200 mg on the scale of measurement. The analysis survey was carried out within the following limits of the measuring systems of the device: DTA = 250 μV, DTG = 500 μV, TG = 500 μV, and T = 500 μV. The results of the analysis were compared with the data from the thermal curves of minerals and rocks given in the atlases and were compared with the descriptions of the thermal behavior of samples set out in other reference sources and accumulated in the databank of the laboratory that conducted these studies.

X-ray phase determinations were carried out on an automated diffractometer DRON-3 with $Cu_{K\alpha}$ radiation and a β-filter (DRON-3, manufacturer: "Burevestnik", Saint-Peterburg, Russia). X-ray phase measurements were performed on a semiquantitative basis using powder sample diffraction patterns via the method of equal weights and artificial mixtures. Quantitative ratios of crystalline phases were determined. Diffraction patterns were interpreted using data from the ICDD file, the powder diffraction database PDF2 (Powder Diffraction File), and diffraction patterns of pure minerals. The content was calculated for the main phases. Possible impurities, the identification of which cannot be unambiguous due to a small number of contents and the presence of only 1–2 diffraction reflexes or poor crystallization, are indicated in the tables.

Along with the traditional classical methods of studying the composition of rocks, in some samples, their elemental and oxide compositions were determined using the method of radiometric microanalysis. The selected samples from different areas were taken with a Superprobe 733 electronic probe microanalyzer from JEOL (Tokyo, Japan). Elemental analysis of samples and photography with various types of radiation were performed using an INCA 8N8RGY energy-dispersive spectrometer from Oxford Instruments (Abingdon, England), which was installed on the above microanalyzer (Superprobe 733) with an acceleration voltage of 25 kV and a probe current of 25 mA.

The involvement of these methods in the study of the material composition of rocks from the pre-salt deposits of the LTCGD made it possible to identify the presence of calcite, dolomite, magnesite, and other minerals that quantitatively vary depending on the depth of occurrence of the rocks.

3. Results

3.1. Results of Macro- and Microscopic Studies

The carbonate reservoirs of the deposit are mainly organogenic-lumpy limestones, which are partially or completely recrystallized and dolomitized; dolomites are substituted for organogenic limestones. In limestones, the shaped elements (lumps and clots) with a size of 0.1–1 mm and an oval, rounded, elongated, or irregular shape are composed of pelitomorphic calcite and are cemented with carbonate material for better crystallization (Figures 4–6).

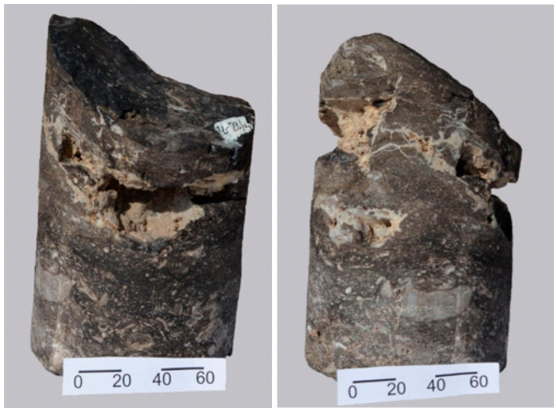


Figure 5. Inclined joint of tectonic separation in Famennian–Carboniferous rocks (detail of Figure 4(3)) with subsequent development of vugginess and new formations of carbonate minerals.

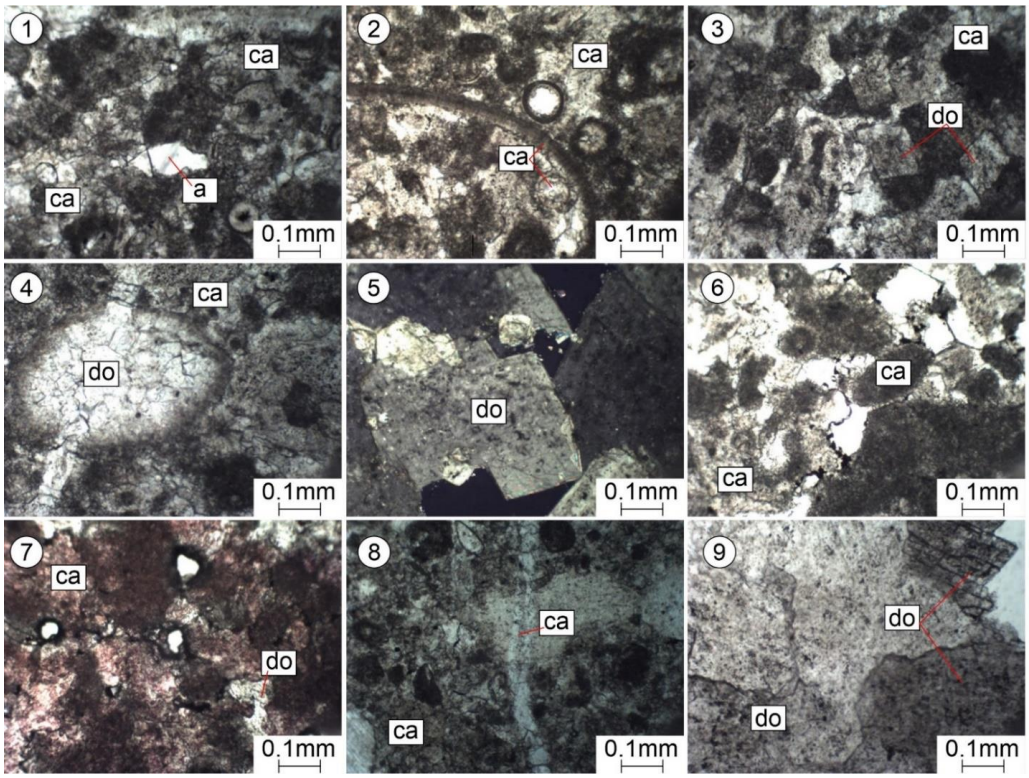


Figure 6. Pictures of thin sections. Epigenetic changes in Famennian–Tournaisian carbonate reservoirs. (**1**–**4**)—organogenic-lumpy limestones, partially recrystallized and dolomitized; depth, 4390 m; Nicole one. (**5**)—crystalline granular dolomite; depth, 4616–4621m; Nikoli +. (**6**)—organogenic-lumpy limestone; depth, 4380 m; Nicole one. (**7**)—organogenic-lumpy limestone (after staining with alizarin red); depth, 4380 m; Nicole one. (**8**)—organogenic-lumpy limestone, slightly recrystallized; depth, 4915 m; Nicole one. (**9**)—crystalline granular dolomite; depth, 4616–4621m; Nicole one.

Carbonate reservoirs are composed of calcite, dolomite, a small amount of barite, anhydrite, pyrite, and clay minerals, in addition to there being a finely dispersed impurity of organic matter, which is sometimes in the form of a film on the surface of carbonates or "effusions" in the core (Figure 4(6). Organogenic residues include ostracods, brachiopods, crinoids, and ammonites composed of fine-grained carbonates. The structure of rocks is organogenic-lumpy and crystal-grained, and the texture is weakly layered or erratic [4,5,12,13]. The rocks are porous, fractured, and cavernous (Figures 4 and 5). Lithogenetic and tectonic joints, as well as stylolites (according to morphology, serrated, and tubercular), are made of clay–organic substance. They are weakened zones along which rocks are split, forming an uneven surface (Figure 4(7,8)). Along the stylolites, there are new formations of large grains of carbonates (calcite, dolomite, and pyrite). These zones are favorable for the formation of open joints.

As a result of the microscopic studies, epigenetic processes of recrystallization, dolomitization, substitution, leaching, and secondary mineral formation were revealed. Sulphate mineralization was noted, which leads to the sealing of voids and thus reduces the porosity of carbonate reservoirs (Figure 6(1)).

In the studied rocks, there are voids formed as a result of the epigenetic leaching of calcite from formed formations (organogenic residues of Crinoidea, ostracods, etc.) (Figure 4(2,4)) of various sizes: from small pores to large caverns of an irregular shape (Figure 5). Pores and caverns are often encrusted with well-formed crystals of rhombohedral dolomite (Figure 6(3,5,9)).

Epigenetic dolomitization: dolomite crystals of a rhombohedral shape are found in the granular mass of calcite (Figure 6(3)) when it is relatively intense and multi-faced rhombohedrons of dolomite are in contact with either edges or vertices with faces (Figure 6(9)). Given such packaging, significant intergranular spaces comparable to grains remain free between them; as a result, the porosity of limestones increases significantly. The pores occupy about 10%, have an angular and irregular shape, are located between the large (up to 1 mm) rhombohedral grains of dolomite, and are mainly isolated (Figure 6(5)). Formations (organogenic fossils) are dolomitized, and some are crossed by a later vein, which indicates a later process of dolomitization (Figure 6(4)).

3.2. Results of Analytical Studies

When dynamically heating the 10-1 sample drawn from the depth of 4616–4621 m, the differential (DTA and DTG) curves showed pronounced endothermic manifestations caused by the reactions and the destruction of the thermally active components of the sample. The morphology of these curves, formed in the range of 495–850 °C, indicates the presence of dolomite, calcite, magnesite, and siderite in the sample, as shown in Figure 7 [14]. Peaks related to the dissociation of the compounds $MgCO_3$, $CaCO_3$, $CaMg(CO_3)_2$, and $FeCO_3$ were reconstructed from these curves based on the total thermal manifestations obtained during the firing process [15–18]. At the same time, the identified temperature intervals, in which the gradual removal of carbon dioxide (CO_2) into the atmosphere was carried out, were determined as weight losses corresponding to the values of 26.3%, 10.35%, 6.5%, and 2.6%. Taking into account these emissions and stoichiometric formulas of these carbonates, the percentage of their content in the sample was established, where the dolomite was 55.1%, calcite was 23.5%, magnesite was 12.5%, and siderite was 6.8% (Table 1).

The X-ray phase analysis of the sample resulted in a curve with a series of diffraction peaks, of which only one (D—2.8842) achieved an intensity acceptable for the identification of the phases present (Figure 7, Table 2). This peak indicates the presence of dolomite in the sample. The remaining diffraction reflexes left very poorly developed peaks on the curve, which may be due to the low content of substances in the sample that caused these dispersed spikes, or due to the presence of poorly crystallized impurity minerals in the rock.

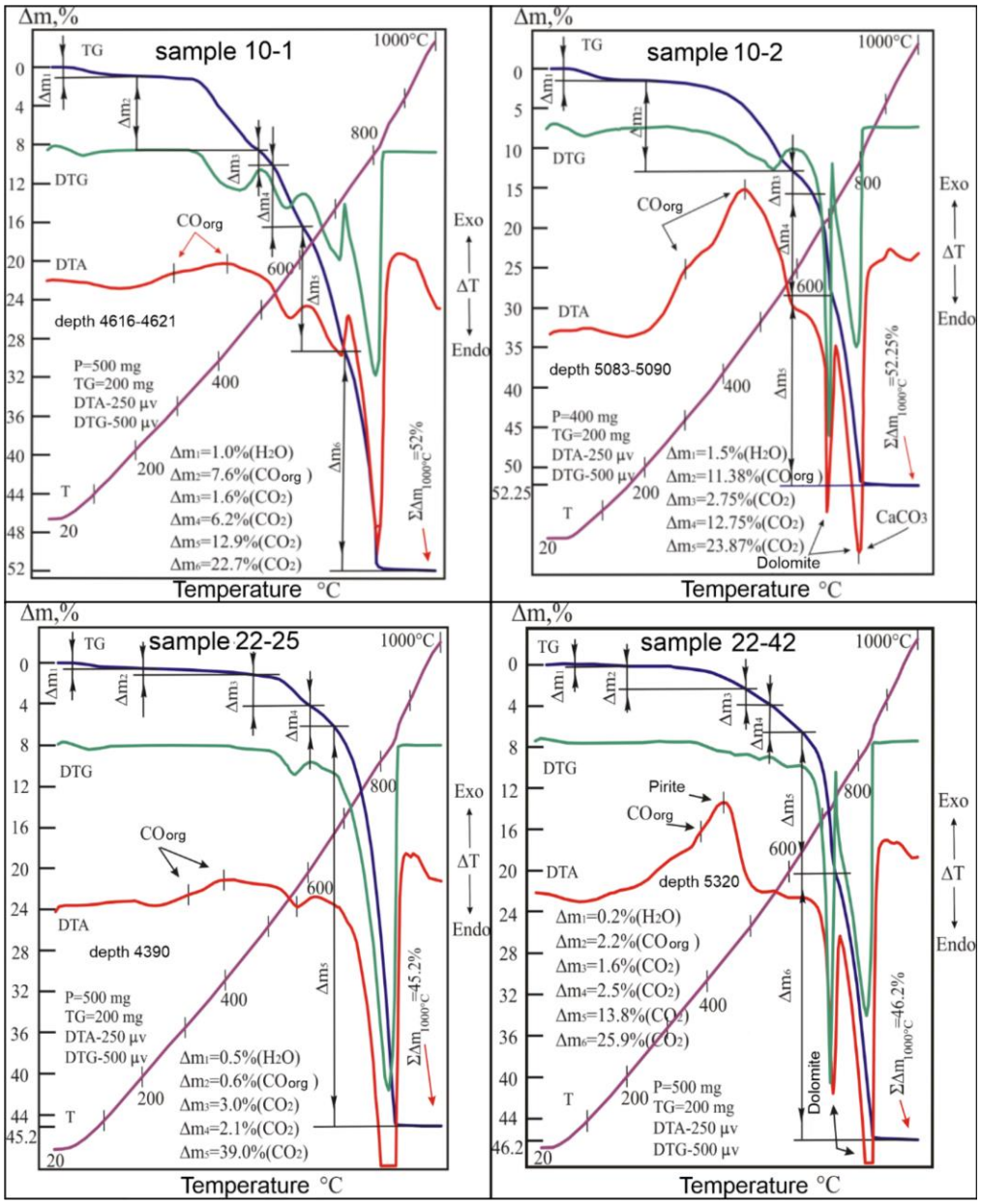


Figure 7. Derivatograms of samples: 10-1, 10-2, 22-25 and 22-42.

The results of the semiquantitative X-ray phase analysis of crystalline phases are shown in Figure 8, and the data of the interplanar distances and the phase composition of the studied sample are summarized in Table 2.

In contrast to the results of the semiquantitative radiometric measurements (Table 2), the thermal analysis found not only dolomite in the sample, but also calcite, magnesite, and siderite in noticeable amounts (Table 1). Thus, the absence of pronounced diffractive reflexes of calcite, magnesite, and siderite on the radiograph (Figure 8) does not mean their complete absence in the sample. These carbonates were not detected through X-ray structural analysis due to the poor perfection of the crystalline structures of their lattices. These minerals, even with significant defects in their structures, practically retain their inherent thermochemical properties and are easily diagnosed by DTA methods. According to the complex (XRD and DTA) measurements, the sample contains well-crystallized dolomite, as well as calcium, magnesium, and iron carbonates and crystalline lattices, which were underdeveloped.

Table 1. Summary table of mineral and material composition of the ChD rocks based on the results of thermal analysis.

Sample	Mineral Composition of Samples, wt %							Compounds Removed from Rocks and Minerals, wt %			LI, 1000 °C
	Depth, m	Dolomite	Calcite	Magnesite	Siderite	Miscellaneous Minerals	Thermally Inert Minerals (TIM)	CO_{org}	H_2O	CO_2	
10-1	4616–4621	55.1	23.5	12.5	6.8	–	2.1 (CaO, MgO)	7.6	1.0	43.4	52.0
10-2	5083–5090	56.0	28.4	2.5	–	Pyrite 1.5	0.5 (CaO, MgO)	11.3	1.5	39.58	52.2
22-25	4390	8.8	83.9	5.7	–	-	0.5 (CaO, MgO)	0.6	0.5	44.1	45.2
22-42	5320	59.5	29.3	4.8	–	Pyrite ~2	2.0 (CaO, MgO)	2.2	0.2	43.8	46.2

Note: LI—loss on ignition.

Table 2. Interplanar distances and sample phase composition of 10-1.

d, Å	I %	Mineral	d, Å	I %	Mineral
4.03153	0.5		2.19195	2.5	dolomite
3.69761	0.6		2.06467	0.4	
3.19480	2.4		2.01492	1.2	
2.97414	0.8	β quartz	1.84720	0.4	dolomite
2.88420	100.0		1.80371	3.1	dolomite
2.66722	2.4	dolomite	1.78564	2.3	
2.53819	1.0		1.78015	1.3	

The 10-2 sample showed a slightly different roasting behavior, which was removed from a deeper depth (5083–5090 m) than the 10-1 sample. However, the thermal degradation of its components is mostly similar to that of the latter, which indicates the similar identity of their material composition. Under the conditions of dynamic heating, the test sample showed on its curves the same bends that were traced on the lines of the above-considered derivatogram, according to Figure 7. Here, the leading role in the formation of analog information about the processes occurring in the system is played by the temperature and chronological parameters that cause the destruction of carbonate formations, and the quality of molecular bonds of H_2O, CO_2, and CO_{org} in the structures of minerals play a part as well. In this system, only one of these compounds, H_2O, when released into the atmosphere, does not carry any significant information about the state of the tested system due to its low content in the sample (1.5%), as there is an absence of links of this water to any crystalline inclusion of the sample.

Reactions traced at higher temperature intervals (645–825 °C) appeared on all derivatogram curves. According to the location of the peaks on the DTA and DTG curves in the test temperature range, and taking into account their amplitudes, which are responsible for the degree of intensity of thermal reactions, it was established that each sample decomposition process belongs to a particular structure.

Thus, according to the mineral accessories of the components of the complex, the differentiation of thermal manifestations was carried out. In the above temperature range, dolomite and calcite are usually decomposed. In dolomite ($CaMg(CO_3)_2$), the destruction process takes place in two stages. First, there is a dissociation of the magnesium component, in which 50% of the existing carbon dioxide is removed from the system; then, there is a decomposition of the calcium component, accompanied by the loss of the remaining

amount of CO_2 (also 50%). Therefore, according to the thermogravimetric data of the sample (Table 3), the weight loss ($\Delta m_3 + \Delta m_5$) caused by the destruction of the specified carbonate in the range of 585–645 and 645–825 °C was 26.9%, and, taking into account its stoichiometric formula, the amount of dolomite in the sample composition corresponds to 56.0% (Table 1).

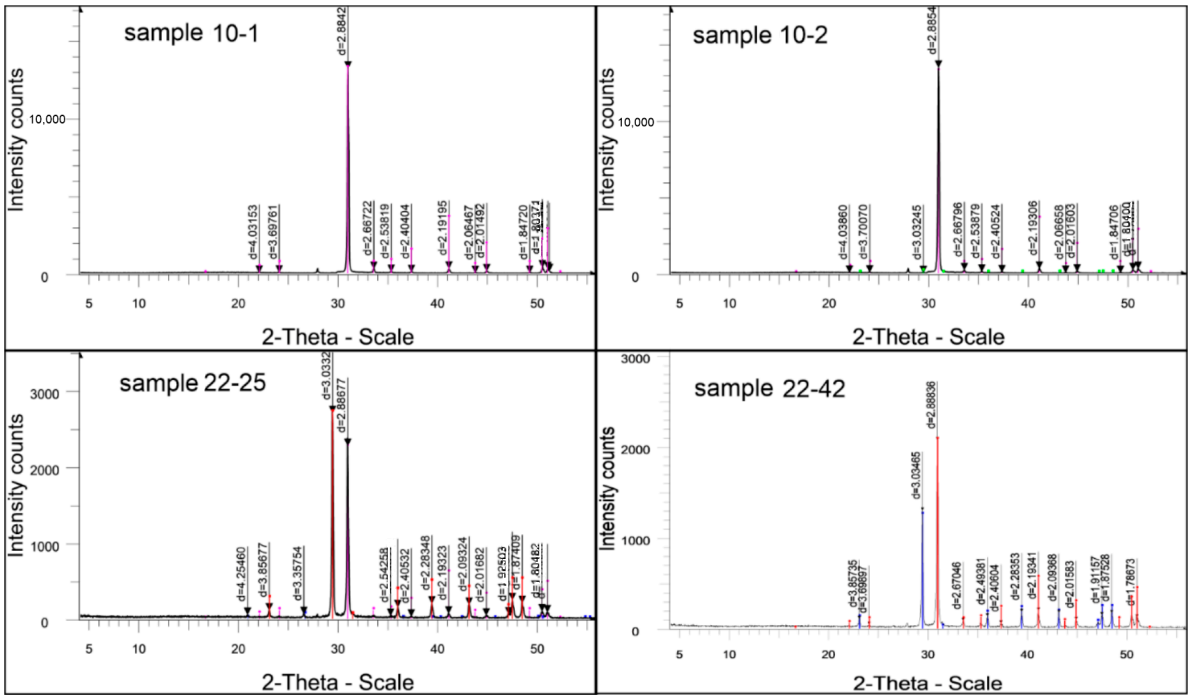


Figure 8. Sample diffraction pattern results of semiquantitative X-ray phase analysis of crystalline phases: 10-1 sample: dolomite $CaMg(CO_3)_2$—99.0%, X-ray amorphous impurities—1%. 10-2 sample: dolomite $CaMg(CO_3)_2$—99.2%; calcite $Ca(CO_3)$—0.8%. 22-25 sample: $Ca(CO_3)$ calcite—53.9%; dolomite $CaMg(CO_3)_2$—44.9%; SiO_2 quartz—1.2%. 22-42 sample: dolomite $CaMg(CO_3)_2$—62.3%; calcite $Ca(CO_3)$—37.7%.

Table 3. Thermogravimetric readings of sample 10-2 in the range of 20–1000 °C.

Weight Loss Sequence	Amount of Weight Loss, %	Volatile Components of the Heated Sample	Decomposition Stage Temperature Range, °C
Δm_1	1.5	H_2O	20–200
Δm_2	11.375	$10(CO_2)_{org} + 1.375(CO_2)$	200–585
Δm_3	2.75	CO_2	585–645
Δm_4	12.75	CO_2	645–705
Δm_5	23.875	CO_2	705–825
$\sum\Delta$m1000 °C	52.25	H_2O, CO_{org}, CO_2	20–1000

The presence of calcite in the sample composition was traced by the endothermic reaction, the temperature limits of which coincided with the stage of decomposition of the calcium component of dolomite. The amount of released carbon dioxide during $CaCO_3$ dissociation was determined based on the difference between the weight loss recorded in the range of 705–825 °C and the weight loss of calcite in the same temperature interval [16]. After corrective procedures for ordering the values of the thermogravimetric parameters (Figure 6), the weight loss of calcite was indicated to be 12.5% (CO_2). Taking into account this value and according to the stoichiometric formula of CaCO3, the calcite content in the sample composition was 28.4% (Table 1).

The main feature explaining the genetic affiliation of the revealed calcite, dolomite, and magnesite is the thermal behavior of the sample containing these minerals. The investigated aggregate under dynamic heating, among other thermochemical properties, indicates the following features of its thermal behavior:

(1) The studied carbonate complex within the temperature range of 600–820 °C decomposes in two stages, leaving on the DTA curve two endothermic peaks of different areas at 700 °C and 800 °C, caused by the effects of destruction first of the magnesium part of dolomite ($MgCO_3$), then calcium ($CaCO_3$) (Figure 7, samples 10-2 and 22-42)

(2) The temperature–chronological parameters of the second stage of dolomite destruction completely coincide with the parameters of decomposition of calcite present in the rock. In this regard, the endothermic effect of the second stage of decomposition of the indicated carbonate complex is caused by the total emissions from the CO_2 system as a result of the decomposition of the calcium component ($CaCO_3$) of dolomite and the simultaneous decomposition of calcite, the mineral component of the studied rock. At the same time, on the DTA curve, the area of the second peak (S_2) exceeds the area of the first (S_1) by more than 1.7 times. The proportionality coefficient 1.7 is borrowed from the ratio of areas (S_2 = 1.7 S_1) of endothermic peaks formed on the DTA curve as a result of the decomposition of pure pure dolomite [17]. Similar kinetics of thermal decomposition of dolomite–calcite formation are characteristic of the carbonate complex, in which the structure of calcite was formed mainly due to the decomposition products of dolomite, i.e., due to the replacement of the magnesium cation in this mineral by calcium.

(3) Thermal parameters of decomposition of carbonates indicated that magnesite and calcite in these associations are secondary minerals in relation to dolomite. The secondary nature of magnesite (samples 10-1 and 22-25) is confirmed by the close location of the temperatures of the endothermic reactions of the destruction of magnesite (mineral) and the magnesium component of dolomite, and the secondary nature of the origin of calcite (samples 10-2 and 22-42) is explained by the coincidence of temperature intervals and time of decomposition of calcite (mineral) and calcium component of dolomite.

(4) Since dolomite in the first stage of decomposition loses 50% of carbon dioxide (Δm_1), and during the passage of the second stage of decomposition, the remaining 50% of carbon dioxide (Δm_2) is removed, then the violation of this balance is in favor of an increase in the release of Δm_2 (CO_2) in the final second part of dissociation due to the presence of calcite in the system. The weight loss dm caused by the degradation of this carbonate is included in the second step of the TG curve, which corresponds to the second step of CO_2 release from the complex under consideration. Using this parameter, it is easy to determine the content of secondary calcite in the composition of the studied rock.

It should be noted that in such mineral associations, where dolomite is primary in relation to calcite, organic compounds (CO_{org}) are often included, the presence of which in the samples is easily established by the exothermic effect manifested in the range of 250–550 °C (Figure 7, samples 10-2 and 22-42). Based on our results, these carbonate associations are characterized by high micro-porosity and fracturing and can be used as criteria in the search for hydrocarbon deposits.

The thermal dissociation of magnesite takes place together with the combustion of the organic matter (OM) present in the sample; i.e., it takes place within the temperature interval that causes the weight to decrease, Δm_2. The proportion of CO_2 emitted by magnesite was 1.375%, which corresponds to the 2.6% presence of this carbonate in the sample. The remainder of the weight loss (10%) was caused by the release of carbon monoxide from the combustion system of the organic compound (Table 1).

Radiometric data of this sample showed that the rock under study mainly consists of dolomite (99.2%) and only 0.8% calcite (Figure 6). Such a discrepancy between the sample composition and the thermal analysis data, as is the case for the 10-1 sample, is due to the presence of poorly developed calcite in the sample. Recording such poorly crystallized calcite in the sample by using the XRD method is difficult (Table 4).

Table 4. Interplanar distances and phase composition of sample 10-2. Note: the test substance in the sample is poorly crystallized.

d, Å	I %	Mineral	d, Å	I %	Mineral
4.03860	0.5		2.40524	0.8	
3.70070	0.7		2.19306	2.5	dolomite
3.19505	2.4	β quartz	2.06658	0.5	
3.03245	0.4	calcite	2.01603	1.1	
2.97326	0.9	dolomite	1.84706	0.4	dolomite
2.88540	100.0		1.80400	1.8	dolomite
2.66796	1.8		1.78664	2.4	

All the given diffraction peaks of the 10-2 sample (Figure 8) belong to the phases listed in Table 4 only. In the X-ray phase analysis of the test sample, characteristic diffraction reflexes are given, allowing for the identification of the phases present.

To control the mineral and material composition of this rock that was identified via the methods of XRD, DTA, and TGA, data on the elemental composition of samples obtained from an electron-probe microanalyzer were used (Tables 5–7, Figure 9).

Table 5. Results of the elemental composition of sample 10-2 obtained from a probe microanalyzer.

Processing Parameters: All Items Analyzed (Normalized)							
All results in weight %							
Spectrum	O	Mg	Si	S	Ca	Fe	Total
Spectrum 1	56.91	14.89	0.22	0.47	27.31	0.20	100.00
Spectrum 2	57.86	14.64	0.24	0.50	26.51	0.25	100.00
Spectrum 3	56.51	14.62	0.34	0.41	27.88	0.24	100.00
Secondary	57.09	14.72	0.27	0.46	27.23	0.23	100.00

Table 6. The 10-2 sample processing parameters: carbon by difference.

All Results in Weight %								
Spectrum	O	Mg	Si	S	Ca	Fe	C	Total
Spectrum 1	44.53	9.20	0.13	0.30	18.19	0.13	27.52	100.00
Spectrum 2	45.79	9.17	0.15	0.32	17.84	0.17	26.56	100.00
Spectrum 3	42.08	8.30	0.19	0.24	17.29	0.15	31.75	100.00
Secondary	44.13	8.89	0.15	0.29	17.77	0.15	28.61	100.00

Table 7. Results of the oxide composition of the 10-2 sample obtained from a probe microanalyzer.

Processing Parameters: Oxygen by Stoichiometry (Normalized)						
All Results in Compounds %						
Spectrum	MgO	SiO2	SO3	CaO	FeO	Total
Spectrum 1	36.32	0.78	1.91	60.58	0.41	100.00
Spectrum 2	36.39	0.88	2.07	60.14	0.53	100.00
Spectrum 3	35.43	1.18	1.65	61.24	0.50	100.00
Secondary	36.05	0.94	1.88	60.65	0.48	100.00

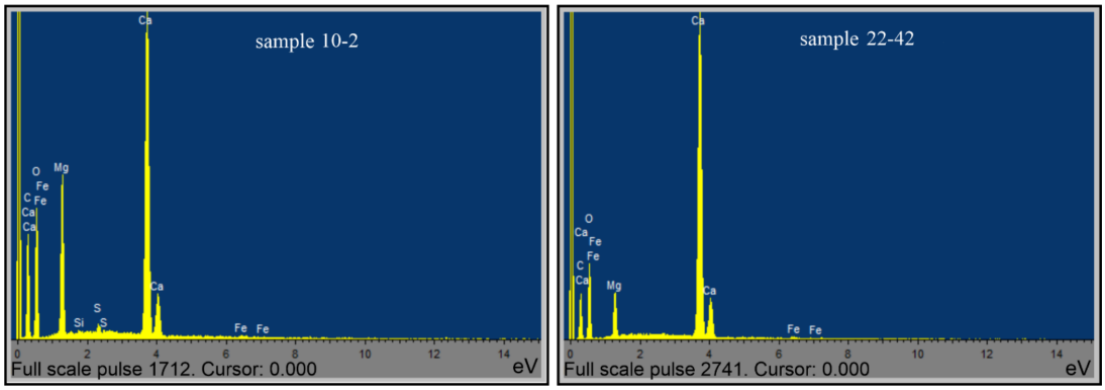


Figure 9. Elemental composition spectrum of samples: 10-2 and 22-42.

The given data of the electron-probe microanalysis on the elemental, oxide, and carboxylic content of the 10-2 sample rock correspond to the composition of minerals established by X-ray diffractometry and the thermal analysis complex (Figure 9). Within the limits of the capabilities of the used scientific equipment, the results obtained are quite acceptable for identifying the degree of perfection of the crystalline structures of carbonate minerals and can be used to determine the mechanism of accumulation and migration of hydrocarbon complexes in the sedimentary strata of the studied massif.

Limestone taken at the depth of 4390.9 m is an aggregate of calcite with impurities of magnesium carbonates. This is evidenced by the results of the thermal analysis of the powder sample from the studied core. Dynamic heating of this sample (22-25) led to the formation of many manifestations on the DTA, DTG, and TG curves due to the thermal destruction of calcite and, to a lesser extent, dolomite and magnesite (Figure 7). Along with these reactions, the thermal curves revealed weak emissions from the water system and organic carbon monoxide, which reduced the sample weight by 0.5 and 0.6%, respectively. Despite the similarity of the sample's composition with that of the 10-2 sample, the thermal behavior of the test sample was still somewhat different from the processes of decomposition of the compared core. This difference can be seen in the absence of an endothermic peak on the DTA curve of the studied system, which is responsible for the mode of destruction of the magnesium component ($MgCO_3$) of dolomite. Instead of said peak on the DTA and DTG curves, a slight deflection was recorded within 600–675 °C, indicating the development of a weak decomposition reaction of said magnesium component of dolomite in the sample. In this case, the thermogravimetric (TG) curve in the interval of the noted temperatures recorded a drop in the sample weight (Δm_4) by 2.1%. The same weight reduction of the sample's 2.1% dolomite was carried out in the range of 675–710 °C. Calcite decomposes simultaneously in the temperature range of 675–860 °C with dolomite (Figure 7). Using the stoichiometric formula of $CaMg(CO_3)_2$ and the amount of carbon dioxide emitted into the atmosphere (2 × 21.1%), it is not difficult to calculate the dolomite content in the system. The amount of it in the rock corresponded to 8.8%. Based on the results of the sample weight loss during the endothermic reactions in the regions of 460 °C and 830 °C, the presence of 5.7% magnesite and 83.9% calcite in the sample was calculated. The content of water and OM in the sample composition was determined based on the stages of weight loss in the temperature ranges of 20–200 °C and 200–460 °C, respectively (Figure 7, Table 1).

The high concentration of calcite (83.9%) in the sample composition made it possible to determine the kinetic constants of thermal dissociation of this carbonate. Using the technique from [18–20], the activation energy (E_A) of the emissions from the carbon dioxide system was calculated. In the process of $Ca(CO_3)$ destruction, the specified parameter was 250 kJ/mol, which corresponds to a high degree of perfection in the crystalline structure of this calcite.

The kinetic calculations also established that the modular value of EA of the studied carbonates is directly dependent on the value of free energy of their structures. Taking into account this regularity and inequality of $E_{A(calcite)} > E_{A(dolomite)}$, it follows that the direction of mineral transformation in calcite–dolomite systems largely depends on the energy levels of their crystalline structures, and then on the geochemical environment of the surrounding space. A sample analysis confirmed this inequality. In turn, the energy parameter of dolomite E_A is composed of the activation energy of the calcium component ($E_{A1}(CaCO_3)$) and its magnesium component ($E_{A1}(MgCO_3)$), i.e., the equality of $E_A(dolomite) = E_{A1}(CaCO_3) + E_{A1}(MgCO_3)$ is met.

It can be seen here that the energy level of the crystalline lattice of mono-mineral calcite is higher than the level at which the dolomite is located. In this regard, according to the Ostwald rule on the energy preference of the transition of one mineral system to another [19,20], the conversion of calcite to dolomite is more likely to occur than the conversion occurring in the opposite direction. This means that during the development of the new phase, the partial substitution of the Ca cation with Mg in the transformable calcite is less difficult than the substitution of magnesium dolomite with calcium. This conclusion is also true for the corresponding carbonates of the LTCGD. The process of converting calcite to dolomite in sediments, together with the introduction of clay minerals into carbonaceous complexes, can be attributed to one of the important stages of the formation of reservoirs and pore spaces (in carbonate strata) with high capacitive and filtration properties [21]. Further, it follows that the (mineral) destruction of $CaCO_3$ requires more energy consumption than the destruction of the dolomite structure. Such a conclusion, which is based on the direction of formation of mineral phases in the calcite of dolomite strata, can be used to identify the dependence of the productive properties of reservoirs not only on the composition of carbonate–clay complexes, but also on the degree of conversion of calcite to dolomite in these associations.

Table 8 lists the unit cell parameters: interplanar distances of the formation under study, d, Å, intensities of reflection, I%, and phase composition. In Figure 8, these parameters correspond to the positions of the peaks and the magnitude of their heights, indicating the composition and amount in the sample. This sample is characterized by the appearance of lines of quartz, β-quartz, dolomite, and calcite in the diffraction pattern.

Table 8. Interplanar distances and phase composition of the 22-25 sample.

d, Å	I %	Mineral	d, Å	I %	Mineral
4.25460	2.2	quartzite	2.40532	1.4	
3.85677	4.4		2.28348	7.7	
3.35754	2.6	β-quartz	2.19323	2.9	
3.19865	2.2	calcite	2.09324	7.1	
3.03324	100.0	dolomite	2.01682	1.9	dolomite
2.88677	84.1		1.92503	2.4	
2.84487	2.9		1.91098	9.4	
2.54258	1.8	dolomite	1.87409	7.9	
2.49272	5.9		1.80482	4.0	

It should be noted that the mineral composition in this rock, according to XRD data, somewhat differs from the material content presented by thermal analysis. Additionally, this is natural, since X-ray diffractometry gives the mineral content only from the crystalline part of the sample, whereas the thermogravimetric method used to determine the mineral composition is carried out relative to the entire mass of the substance under study, i.e., relative to the crystalline and amorphous parts of the sample. In addition, the presence of various salts and thermally inert disperse formations in the system under study can partially change the kinetics of the thermal decomposition of carbonates, which also

leads to interference with the reliable determination of the quantitative content of mineral phases [18].

The 22-42 sample, which is from the lower stratigraphic level (5320 m), was heated via continuous temperature increase. This caused the 22-42 sample to leave a series of endo- and exothermic orientations on the thermal curves (Figure 7). The differential thermoanalytical (DTA) and differential thermogravimetric (DTG) curves in the range of 625–825 °C formed their trajectories in a W-shaped curve, which corresponds to the endothermic peaks of the thermal decomposition of dolomite. The depths of these peaks during $CaMg(CO_3)_2$ dissociation are usually the same. However, in the case under consideration, the value of the second peak (at 830 °C) was slightly higher than the value of the first one, which is due to the presence of calcite in the composition of the dolomite formation, the endothermic peak of which is also located at 830 °C. According to the thermogravimetric (TG) curve, it was found that when the dolomite dissociates into the atmosphere, a series of CO_2 molecules rush in (in two stages) with a mass of 28.4%, corresponding to the weight loss of the sample in the temperature interval under consideration. In turn, with the decomposition of calcite, the emission of carbon dioxide leads to a decrease in the weight of the sample by another 12.9%. Using these values to calculate the mineral content of the rock with TG determinations and stoichiometric formulas, the presence of dolomite (59.5%) and calcite (29.3%) was found in the sample.

According to the thermal effects recorded on the DTA curve in the range of 20–220 °C, the sample was found to be dehydrated with a weight loss of 0.2%, and for that in the range of 220–640 °C, the reaction of burning organic matter (CO_{org}) with a decrease in the sample weight of 2.2% was established. On the same curve, a pronounced exothermic peak with a vertex at 440 °C was noted. The effect was caused by the oxidation of pyrite along with the formation of hematite (α-Fe_2O_3) [17,18]. The amount of sulfide (FeS_2), counted in the peak area, corresponds to 2%. Finally, the presence of magnesite in the sample was detected from the weak endothermic dip of the DTA curve in the range of 550–640 °C. Within these temperatures, the TG line recorded a sample weight loss of 2.5%, which corresponds to a magnesite content of 4.8%. The parametric data of these reactions and information on the mineral and material composition of the rock are given in Table 1.

The results of the X-ray structural analysis are presented in Table 9, and the diffractometric reflexes of the test sample are reflected in the diffractogram in Figure 6. All diffraction peaks listed here belong to the above phases only. Characteristic diffraction reflexes are also noted, allowing for the identification of the phases present.

Table 9. Interplanar distances and phase composition of sample 22-42.

d, Å	I %	Mineral	d, Å	I %	Mineral
3.85735	5.4		2.19341	9.7	
3.69897	2.2		2.09368	8.6	calcite
3.36081	1.8	calcite dolomite	2.06347	1.8	
3.19855	3.0		2.01583	4.8	
3.03465	62.7		1.92592	3.5	
2.88836	100	calcite	1.91157	7.4	
2.67046	43		1.87528	8.5	
2.54064	2.9		1.84784	1.6	
2.49381	6.7		1.80471	7.1	
2.40604	3.0		1.78673	6.1.	dolomite

The control results of the elemental composition of the 22-42 sample, obtained by using the electron-probe microanalyzer, also revealed the correspondence of the mineral composition of the sample obtained via the X-ray and DTA methods (Tables 10–12, Figure 8).

Table 10. Electron-probe microanalysis results, Sample 22-42.

Processing Parameters: All Items Analyzed (Normalized)					
All results in weight %					
Spectrum	O	Mg	Ca	Fe	Total
Spectrum 1	57.58	6.43	35.52	0.47	100.00
Spectrum 2	56.98	5.28	37.49	0.25	100.00
Spectrum 3	57.49	6.71	35.45	0.35	100.00
Secondary	57.35	6.14	36.15	0.36	100.00

Table 11. Results of the oxide composition of sample 22-42 made on a probe microanalyzer.

Processing Parameters: Oxygen by Stoichiometry (Normalized)				
All Results in Compounds %				
Spectrum	MgO	CaO	FeO	Total
Spectrum 1	16.96	82.02	1.02	100.00
Spectrum 2	13.83	85.62	0.55	100.00
Spectrum 3	17.61	81.62	0.77	100.00
Secondary	16.13	83.09	0.78	100.00

Table 12. Processing parameters: carbon by difference.

All Results in Compounds %						
Spectrum	O	Mg	Ca	Fe	C	Total
Spectrum 1	47.61	4.59	27.30	0.36	20.14	100.00
Spectrum 2	45.46	3.57	27.75	0.19	23.02	100.00
Spectrum 3	48.17	4.90	27.72	0.28	18.94	100.00
Secondary	47.08	4.35	27.59	0.27	20.70	100.00

It should be noted that out of all the diversity within the material composition of the rocks, which is represented by carbonates, clays, siliceous formations, and other impurities, OM was also found in the studied wells. In limestones, where the amount of calcite exceeded 96%, the content of the organic compound varied within 0.3%–0.7%. In other rocks, where dolomite, magnesite, and siderite were present along with calcite, the concentration of OM reached 13 percent or more. The increased content of organic matter in these rocks is caused by the presence of a wider range of carbonate–clay minerals and silicon oxides necessary for the formation of reservoirs and pore spaces in the strata.

4. Discussion

The giant Karachaganak oil and gas condensate field located in the northern border zone of the Caspian Basin lies within the Lower Permian–Carboniferous–Upper Devonian carbonate bioherm platform and is oriented in the latitudinal direction with a length of 30 km; the width in the meridional direction varies along the strike from 15 to 5 km and a height of 1.7 km. The reservoir is a massive gas condensate. The productive horizons are composed of biohermic and biomorphic–detritic limestones and dolomites, which have transient differences. Reservoirs of pore and pore-cavern types are identified here, whereas

reservoirs of the fracture type are insufficiently studied [1,2,4–8]. The Kashagan carbonate platform, located in the southern part of the Caspian Basin, was formed between the Visean and Bashkirian stages. The porosity in the interior of the platform is heterogeneous due to the superimposition of dissolution, grouting, and compaction processes. Complex diagenetic evolution led to the formation of mature matrix porosity within the platform and heterogeneous porosity due to the development of large, cavernous pores and joints [12].

An analysis of the literary sources on some oil- and gas-bearing areas within the ancient cratons of the world [22–28] makes it possible to carry out a comparative description of the areas of the LTCGD within the northern marginal zone of the Caspian Syneclise of the East European Craton.

In the Tarim and Sichuan Basins of China, similar diagenetic transformations and karst processes are present in the carbonate rocks, and the presence of fracturing has also been established [23–27]. The results of these works are argued and substantiated through modern methods of petrophysical studies. The development and evolution of porosity in dolomite reservoirs primarily reflect the complex effect of the dissolution and precipitation of minerals in the process of dolomitization [22,25].

In the northeastern part of the African Craton, the area within the Gulf of Suez and the area of the Nile Delta of Egypt, the effective porosity, matrix gas permeability, and reservoir quality parameters were measured in various oil and gas fields [26].

In the Gulf of Suez, at the Oktyabrskoye field (African Craton), a carbonate reservoir has been established [27]. On the basis of a facies analysis, the conditions of sedimentation and petrophysical characteristics of the Turonian Wata Formation were established.

In the South American Craton, the São Francisco do Sul area of Brazil, diagenetic processes control a zone of high permeability in carbonate rocks [28].

In all the above cases, a different instrumental–analytical research base was used.

The capabilities of the proposed integrated method for macro- and microscopic analysis of thin sections and core, X-ray diffraction analysis, DTA, TGA, and microprobe were not used. This technique has shown its effectiveness in studying the digenetic transformations of the reservoir carbonate reservoirs of the Famennian–Tournaisian reservoirs of the Northern marginal zone of the Caspian Syneclise.

The LTCGD are located above the protrusion of the Proterozoic basement [5,8]. Two genetic types of reservoirs were identified: (1) porous and pore-cavernous types and (2) joints (shear zones). It has been established that organogenic limestones are characterized by processes of recrystallization, dolomitization, substitution, leaching, and secondary mineral formation. The photos of the thin sections show various types of organogenic–lumpy limestones that are recrystallized and dolomitized to varying degrees (Figure 6). Often, as a result of post-sedimentation transformations, the rock completely loses its organogenic structure and acquires a crystalline structure, becoming relict–organogenic. In such cases, the primary structure is determined by relics and contours of organic fossils or by the relative arrangement of crystals of different sizes and orientations. Various stages of recrystallization can be traced in the thin sections of organogenic limestones, the photos of which are shown in Figure 6, where the cement and skeleton of the remains of organisms underwent recrystallization but retained their shape. Along with further recrystallization, the relics of the primary organogenic–lumpy structure are preserved in the form of a characteristic distribution of crystals of various sizes.

The staging of post-sedimentation processes is shown in Figure 6, where it is expressed via the following sequence: first, the incomplete recrystallization of the primary calcite mass, then uneven dolomitization, then leaching of the unchanged residual calcite and filling in the intercrystalline pores with anhydrite, and somewhat later, selective leaching of the rock with the formation of voids of several centimeters. The intensive manifestation of the dissolution and leaching processes led to the formation of large pore–cavernous cavities that are several centimeters in size.

Epigenetic mineral, texture-structural transformations of carbonate rocks, expressed through the recrystallization of carbonates and the emergence of a secondary joint–pore

space in rocks, can be traced in Famennian–Carboniferous carbonates. The main rock-forming minerals are calcite, dolomite, and magnesite. Minor minerals are represented by siderite, rhodochrosite, manganocalcite, clay formations (kaolinite, hydromica, and mixed-laminated minerals), iron sulfides, magnesium, silicon, and calcium oxides.

5. Conclusions

The final formation of the reservoir properties of carbonate rocks occurred as a result of the development of tectonic fracturing and the diagenetic processes of leaching and secondary mineral formation. According to the data of the microscopic investigation, fracturing, stylolitization, and leaching increase the permeability and porosity of carbonate rocks. Epigenetic recrystallization, dolomitization, and sulfatization have a significant impact, worsening the reservoir properties of rocks in this case. On the contrary, tectonic fracturing contributes to an increase in pore space.

Based on the results of X-ray diffractometry (X-ray), thermal analysis (DTA and TGA), probe microanalysis, and complex microscopic study of Famennian–Tournaisian carbonate rocks of the LTCGD, their mineral and material composition was determined. The rocks were composed mainly of forms of calcite with crystalline lattices at different degrees of perfection, dolomites with moderately ordered structures, and magnesites with underdeveloped bonds of carbon dioxide in the intermolecular space.

Among these instrumental methods, a special place was given to thermal analysis. It was used to study the kinetics of thermal destruction of the $Ca(CO_3)$ and $CaMg(CO_3)_2$ structures, on the basis of which the scheme for the formation of dolomite due to the decomposition products of calcite and vice versa was established. It was found that most of the samples from dolomite–calcite associations contain calcite, the destruction of which requires the expenditure of higher activation energies (E_A) than is seen in the structures of dolomites. Thus, according to the Ostwald rule, the energy level of crystal lattices of similar calcites is higher than that of dolomite structures. In this regard, calcites in these associations are easily transformed into dolomites by partial replacement of the calcium cation with magnesium. Vice versa, if the energy level of the calcite crystal lattice is equal to or lower than the level of dolomite, then the transformation goes in the opposite direction: from the dolomite phase to the formation of the calcium carbonate structure. The interpretation of these data showed that in the studied carbonate sequences, the transformation of calcite into dolomite is more preferable than the reverse transformation.

As a result of comparing the activation energy of the ($E_{A1}(CaCO_3)$) decomposition of the calcite part of dolomite with the activation energy of $E_{A2}(CaCO_3)$ as it related to the dissociation of calcite proper, it was found that the value of $E_{A2}(CaCO_3)$ exceeds the values of $E_{A1}(CaCO_3)$. The calculations also showed that the activation energy of calcium decomposition of the containing component ($E_{A1}(CaCO_3)$) of dolomite was higher than the activation energy of the magnesium component of dolomite.

The interpretation of these data showed that in the studied carbonate strata, the transformation of calcite into dolomite is preferable to the reverse transformation. The results of X-ray, DTA, and TGA measurements and data from the probe microanalysis made it possible to identify thermally inert formations in the composition of carbonates as oxides of calcium, magnesium, silicon, iron, and other compounds accumulated during the conversion of carbonates.

On the basis of the conducted studies, an assessment of epigenetic changes in carbonate rocks was made. A comprehensive method for studying the properties of carbonate reservoirs has been proposed and justified, which opens up the possibility of using the applied methods for subsequent studies.

When studying hypergeneous transformations of nickel-bearing weathering crusts of the Kepirsay ultramafic massif, we applied a research technique (X-ray diffractometry for the solid phase of rocks, DTA, TGA), which showed its effectiveness [20]. When studying the Famennian–Tournaisian reservoirs of the northern marginal zone of the Caspian Syneclise in combination with macro/microscopy and a probe microanalyzer, the

material composition and nature of epigenetic changes were determined, and data on the void space of reservoir carbonate reservoirs were obtained.

Our applied methodology is the scientific novelty of this work. We substantiated a rational, relatively inexpensive express method via the testing of samples from carbonate reservoirs.

Author Contributions: Conceptualization, V.K., A.C., Z.T., I.S. and Y.D.; methodology, V.K.; investigation, V.K., I.S. and Y.D.; resources, V.K., I.S. and Y.D.; writing—original draft preparation, V.K., I.S. and Y.D.; writing—review and editing, V.K., A.C., Z.T., I.S. and Y.D.; visualization, A.C., Z.T., I.S. and Y.D.; supervision, V.K.; project administration, V.K.; funding acquisition, V.K., A.C., Z.T., I.S. and Y.D. All authors have read and agreed to the published version of the manuscript.

Funding: This research was funded by the Ministry of Education and Science of the Republic of Kazakhstan (project IRN, grant number AP09260097, contract number no. 177/36-21-23, dated 15 April 2021) and actively supported by the leadership of the Kazakh–British Technical University (Almaty, Kazakhstan). The authors of this article are very grateful for the support provided.

Data Availability Statement: The data presented in this study are available on request from the corresponding author.

Acknowledgments: This research was supported by the leadership of the Kazakh–British Technical University (Almaty, Kazakhstan). The authors thank the reviewers for valuable comments and are grateful to the editor for careful editing.

Conflicts of Interest: The authors declare no conflict of interest.

References

1. Akchulakov, U.; Zholtayev, G.; Iskaziyev, K.O.; Kovrizhnyh, P.N.; Kuandykov, B.M.; Ogay, Y.K. *Atlas of Oil and Gas Bearing and Prospective Sedimentary Basins of the Republic of Kazakhstan*; Kazakshan Institute of Oil and Gas: Almaty, Kazakhstan, 2015; p. 97. (In Russian)
2. Vocalevskiy, E.S.; Bulekbayev, Z.E.; Iskuzhiyev, B.A.; Kamalov, S.M.; Korstyshevsky, M.N.; Kuandykov, B.M.; Kuantayev, N.E.; Marchenko, O.N.; Shudayev, K.S.; Matloshinsky, N.G.; et al. *Oil and Gas Field. Kazakhstan. Reference book*, 3rd ed.; Institute of Geological Sciences Named after K.I. Satpayev: Almaty, Kazakhstan, 2016; p. 409. (In Russian)
3. Bosikov, I.I.; Klyuev, R.V.; Tekiev, M.V. Analysis of spatial distribution of chemical elements of apatite-stafelite ore. *Geol. Geoph. Russ. South* **2021**, *11*, 137–157. (In Russian) [CrossRef]
4. Bagrintseva, K.; Dmitrievsky, A.; Bochko, R. *Atlas of Carbonate Reservoirs of Oil and Gas Fields of East European and Siberian Platforms*; Moscow: Moscow, Russia, 2003; p. 264. Available online: https://www.geokniga.org/books/14853 (accessed on 2 October 2022). (In Russian)
5. Fortunatova, N.K.; Kartseva, O.A.; Baranova, A.V.; Agafonova, G.V.; Offman, I.P. *Atlas of Structural Components of Carbonate Rocks*; VNIGNI: Moscow, Russia, 2005; p. 440. (In Russian)
6. Fortunatova, N.K.; Varlamov, A.I.; Kanev, A.S.; Poroskun, V.I.; Baranova, A.V.; Bushuyeva, M.A. Structure and assessment of the oil potential of carbonaceous carbonate-siliceous Domanik deposits in the Volga–Ural oil and gas province. *Rus. Geol. Geoph.* **2021**, *62*, 929–946. [CrossRef]
7. Daukeyev, S.Z.; Abdullin, A.A.; Bespayev, K.A.; Vocalevskiy, E.S. *Forecast Map of Oil and Gas Potential of Kazakhstan. M 1:2500000*; Ministry of Energy and Mineral Resources of the Republic of Kazakhstan: Almaty, Kazakhstan, 2000. (In Russian)
8. Daukeyev, S.Z.; Vocalevskiy, E.S.; Shlygin, D.A.; Piliphosov, V.M.; Paragulgov, K.K.; Kolomiyic, V.P.; Komarova, V.P. *Deep Structure and Mineral Resources of Kazakhstan (Part 2—Eastern Kazakhstan), Oil and Gas*; National Academy of the Sciences of the Reublic of Kazakhstan: Almaty, Kazakhstan, 2002; p. 248. Available online: https://www.geokniga.org/books/11437 (accessed on 1 November 2022).
9. Iskaziyev, K.O. *Strategy for the Development of Oil and Gas Resources in the Subsalt Deposits of the North of the Caspian Syneclise*; Abstract of the dissertation for a Doctor of Geological and Mineral Sciences; Gubkin Russian State University of Oil and Gas (National Research University): Moscow, Russia, 2021.
10. Zholtayev, G.Z.; Nikitina, O.I.; Zhaymina, V.Y.; Seitmuratova, Y.Y.; Pirogov, T.Y.; Ivanova, N.I.; Fazylov, Y.M.; Musina, Y.S.; Nigmatova, S.A.; Baishashov, B.U. *Modernization of the Phanerozoic Stratigraphic Schemes of Kazakhstan Based on the International Chronostratigraphic Scale—2016–2021*; Institute of Geological Sciences Named after K.I. Satpayev: Almaty, Kazakshan, 2021; p. 139.
11. Mitchell, J. A note on a method of staining to distinguish between calcite and dolomite. In *Colonial Geology and Mineral Resources*; H.M. Stationery Office: London, UK, 1956; p. 182.
12. Ronchi, P.; Ortenzi, A.; Borromeo, O.; Claps, M.; Zempolich, W.G. Depositional setting and diagenetic processes and their impact on the reservoir quality in the late Visean–Bashkirian Kashagan carbonate platform (Pre-Caspian Basin, Kazakhstan). *AAPG Bull.* **2010**, *94*, 1313–1348. [CrossRef]

13. Demeyeva, M.S. Features of formation of carbonate reservoirs at the Chinarevskoye field. *Eng. Sol. Oil Gas. Ind. Kaz.* **2020**, *6*, 130–135.
14. Ivanova, V.P.; Kasatov, B.K.; Krasavina, T.N.; Rozinova, Y.L. *Thermal Analysis of Minerals and Rocks*; Nedra: Leningrad, Russia, 1974; p. 398.
15. Feklichev, V.G. *Diagnostic Constants of Minerals*; Nedra: Moscow, Russia, 1989; p. 479.
16. Tsvetkov, A.I.; Vallashikhina, E.P.; Piloyan, G.O. *Differential Thermal Analysis of Carbonate Minerals*; Nauka: Moscow, Russia, 1964; p. 167.
17. Bondarenko, I.I.; Samatov, I.B. New in the study of siderites. *Izv. Akad. Nauk. KazSSR, Geol. Ser.* **1982**, *1*, 59–62.
18. Samatov, I.B.; Urumbaev, B.U. Thermochemical features of calcite-dolomite formations (on the example of Central Kazakhstan). *Geol. Kaz. Ser. Geol.* **1997**, *2*, 49–56.
19. Coats, A.P.; Redfern, J.P. Kinetic parameters of thermogravime data. *Nature* **1964**, *201*, 68. [CrossRef]
20. Korobkin, V.; Samatov, I.; Chaklikov, A.; Tulemissova, Z. Peculiarities of dynamics of hypergenic mineral transformation of nickel weathering crusts of ultramafic rocks of the Kempirsay group of deposits in Western Kazakhstan. *Minerals* **2022**, *12*, 650. [CrossRef]
21. Putnis, A.; McConnell, J.D.C. *Principles of Mineral Behaviour*; Elsevier: Amsterdam, The Netherlands, 1980; Available online: https://books.google.kz/books/about/Principles_of_Mineral_Behaviour.html?id=v9CzAAAAIAAJ&redir_esc=y (accessed on 4 November 2022).
22. Jiu, B.; Huang, W.; Mu, N.; Hao, R. Petrology, mineralogy and geochemistry of Ordovician rocks in the southwest of Tarim Basin, implications for genetic mechanism and evolution model of the hydrothermal reformed-paleokarst carbonate reservoir. *Mar. Pet. Geol.* **2022**, *140*, 105687. [CrossRef]
23. Chen, L.; Zhang, H.; Cai, Z.; Hao, F.; Xue, Y.; Zhao, W. Petrographic, mineralogical and geochemical constraints on the fluid origin and multistage karstification of the Middle-Lower Ordovician carbonate reservoir, NW Tarim Basin, China. *J. Pet. Sci. Eng.* **2022**, *208*, 109561. [CrossRef]
24. Shi, J.; Zhao, X.; Pan, R.; Zeng, L.; Luo, W. Natural fractures in the deep Sinian carbonates of the central Sichuan Basin, China: Implications for reservoir quality. *J. Pet. Sci. Eng.* **2022**, *216*, 110829. [CrossRef]
25. Yang, L.; Yu, L.; Chen, D.; Liu, K.; Yang, P.; Li, X. Effects of dolomitization on porosity during various sedimentation-diagenesis processes in carbonate reservoirs. *Minerals* **2020**, *10*, 574. [CrossRef]
26. Abuamarah, B.A.; Nabawy, B.S. A proposed classification for the reservoir quality assessment of hydrocarbon-bearing sandstone and carbonate reservoirs: A correlative study based on different assessment petrophysical procedures. *J. Nat. Gas Sci. Eng.* **2021**, *88*, 103807. [CrossRef]
27. Kassem, A.A.; Osman, O.A.; Nabawy, B.S.; Baghdady, A.R.; Shehata, A.A. Microfacies analysis and reservoir discrimination of channelized carbonate platform systems: An example from the Turonian Wata Formation, Gulf of Suez, Egypt. *J. Pet. Sci. Eng.* **2022**, *212*, 110272. [CrossRef]
28. La Bruna, V.; Bezerra, F.H.R.; Souza, V.H.P.; Maia, R.P.; Auler, A.S.; Araujo, R.E.B.; Cazarin, C.L.; Rodrigues, M.A.F.; Vieira, L.C.; Sousa, M.O.L. High-permeability zones in folded and faulted silicified carbonate rocks—Implications for karstified carbonate reservoirs. *Mar. Pet. Geol.* **2021**, *128*, 105046. [CrossRef]

Disclaimer/Publisher's Note: The statements, opinions and data contained in all publications are solely those of the individual author(s) and contributor(s) and not of MDPI and/or the editor(s). MDPI and/or the editor(s) disclaim responsibility for any injury to people or property resulting from any ideas, methods, instructions or products referred to in the content.